RSC Advances

PAPER

View Article Online
View Journal | View Issue

Cite this: *RSC Adv.*, 2020, **10**, 36042

Electrochemical synthesis of tin plasmonic dendritic nanostructures with SEF capability through *in situ* replacement

Jun Dong,*[a] Feifei Wu,[a] Qingyan Han,[a] Jianxia Qi,[a] Wei Gao,[a] Yongkai Wang,[a] Tuo Li,[a] Yi Yang[a] and Mengtao Sun*[b]

Received 26th July 2020
Accepted 21st September 2020

DOI: 10.1039/d0ra06483a

rsc.li/rsc-advances

Dendrite nanostructures with noble metals, such as Au and silver, act as plasmonic substrates with excellent potential in enhanced fluorescence technology. However, tin dendritic nanostructures are poorly investigated. In this study, we proposed a method of *in situ* electrochemical synthesis replacement to fabricate highly branched tin dendritic nanostructures on aluminum substrates. The surface enhanced fluorescence performance of the tin dendrites was tested for the detection of rhodamine 6G as probe molecules, and the result showed that the enhancement factors can reach to 36.5-fold that of an aluminum substrate. The fabricated tin dendrites have numerous nanogaps between the stratified and adjacent ones, thereby creating many plasmon-active "hotspots" dedicated to enhanced fluorescence. Electrical field simulation results for the tin dendritic nanostructures proved that its nanogaps can enhance the nearby local electromagnetic field. As a result, tin dendritic nanostructures exhibit outstanding surface enhanced fluorescence and promising application in biomolecule detection and sensor devices.

1. Introduction

When excited by an external electric field, plasmonic nanostructures can manipulate the light field on the nanoscale and thus have received great attention in catalysis, surface enhanced Raman scattering (SERS), and surface enhanced fluorescence (SEF).[1–5] SEF is one of the most important spectroscopic detection technologies and widely used in various fields such as bioassays, medical research, and photoelectric sensing.[6–10] A highly sensitive fluorescence spectroscopy platform provides good development for fluorescence spectroscopy.[11] Noble metal nanostructures with various morphologies and excellent plasmonic characteristics are widely used in SEF and related areas. Zhang *et al.*[12] reported that 3D flower-like silver nanostructures can be applied as surface enhanced fluorescence substrates that can achieve the largest enhancement factor (EF) of 181. In addition, silver gel film[13] and silver dendritic[14] nanostructures also show good enhanced fluorescence effect. Although, conventional SEF substrates are mostly Ag, Au and Cu,[15–18] Prof. Geddes[19] first reported the enhanced fluorescence effect of tin nano-films prepared through thermal vapor deposition. With the increasing demand for the detection of low-concentration target molecules in a complex environment, developing an enhanced substrate with excellent plasmonic characteristic is important in the investigation. Actually, metallic dendritic nanostructures with multiple fractal structures, hierarchical self-similarity and peculiar optical response characteristics are widely used in various fields, such as solar energy storage,[20] biomedical application,[21,22] and spectroscopy.[23] Moreover, metallic dendrites have many multi-level branched nanostructures, which allow a larger specific surface area. The corresponding complex nanostructures may be more conducive to the absorption of probe molecules,[24] which have significant development in the field of detection. Silver or silver/gold alloyed dendritic nanostructures are being investigated for their potential application in catalysis and SERS.[25,26] When studying the surface-enhanced fluorescence of metal dendritic nanostructures, silver dendritic nanostructures are mainly used to adjust the fluorescence signal.[27] Here, we used a simple and rapid method to prepare tin dendritic nanostructures and investigated the effect of tin dendrites on fluorescence regulation.

In this work, conventional metal tin instead of gold or silver was used to study its enhanced effect. Tin dendritic fractal nanostructures on aluminum (Al) were successfully prepared *via in situ* chemical reaction between $SnCl_2$ solution and Al. In addition, the SEF performances of the tin dendrites were investigated for the detection of rhodamine 6G (Rh6G) as probe molecules. Tin dendritic nanostructures with different sizes and morphologies were generated by changing the reaction time and exhibited various enhanced fluorescence phenomena.

[a]*School of Electronic Engineering, Xi'an University of Posts and Telecommunications, Xi'an, 710121, China. E-mail: dongjun@xupt.edu.cn*

[b]*School of Mathematics and Physics, Beijing Key Laboratory for Magneto-Photoelectrical Composite and Interface Science, Center for Green Innovation, University of Science and Technology Beijing, Beijing, 100083, China. E-mail: mengtaosun@ustb.edu.cn*

The morphology of tin dendritic nanostructures with good enhancement effect and strong stability was simulated and theoretically analyzed. The results show that the tin dendrites on SEF-active substrates with good reliability and reproducibility can contribute to the practical applications of fluorescence detection in biomolecule discovery.

2. Experimental section

2.1 Chemical reagents and materials

All reagents used were of analytical grade. Stannous chloride dihydrate ($SnCl_2 \cdot 2H_2O$) and ethanol (C_2H_6O) were purchased from Sinopharm Chemical Reagent Co., Ltd. (Beijing, China). Aluminum foil (99.9995%) was obtained from Beijing Institute of Nonferrous Metals and Rare Earths. Rhodamine 6G (Rh6G, laser grade) was acquired from Exciton (USA).

2.2 Apparatus

The samples were characterized by scanning electron microscopy (SEM, Carl Zeiss-Sigma), energy dispersive X-ray spectroscopy (EDS), and EDS elemental mapping. Green light was excited by a 532 nm laser as an excitation source. Fluorescence spectrometer (ocean optics) was used to measure the enhanced fluorescence spectrum. COMSOL Multiphysics software is used to simulate the sample.

2.3 Fabrication of tin dendrites on aluminum substrate

The tin dendritic nanostructure was prepared on aluminum substrate through *in situ* replacement. First, weigh 0.034 g of $SnCl_2 \cdot 2H_2O$ crystals and dissolve it in ethanol solution to obtain a concentration of 0.5×10^{-2} mol L^{-1} $SnCl_2$–ethanol solution. Second, the aluminum substrate was polished with an 800 mesh sandpaper for 3 minutes, ultrasonically cleaned with ethanol, and dried using N_2. Finally, the aluminum substrate with length of 1 cm and width of 0.5 cm was cut and placed in $SnCl_2$ solution. At room temperature about 25 °C, the tin dendritic substrates with different morphologies were prepared by adjusting the reaction time. The reaction process was similar to a simple galvanic displacement. The metals transferred the electrons to reduce Sn^{2+} ions and form Sn atoms, which aggregated and grew into dendrites as shown in Fig. 1. Different morphologies of tin dendritic nanostructure were formed by changing the reaction time.

2.4 Investigation of the surface enhanced fluorescence performance

Solutions of Rh6G with different concentrations (10^{-6}, 10^{-7}, 10^{-8}, and 10^{-9} mol L^{-1}) were prepared in ethanol. The prepared tin dendritic substrate was immersed in Rh6G solution for 25 min, and Rh6G molecules formed a uniform film on the sample surface. In the spectrum test, the confocal microscopy light path is used, the sample is under the objective lens, and the fiber optic spectrometer is used to receive the feedback fluorescence signal, and the fluorescence spectrum is displayed on the computer through the CCD. It should be noted that a 532 nm filter should be placed in front of the fiber spectrometer to eliminate the influence of the 532 nm laser on the feedback fluorescence signal. The same 50× microscope objective with an integration time of 0.1 s and a laser power of 5 mW was used for the fluorescence spectrum detection. Spectral testing needs to be carried out in a dark room to reduce the background light. The tested sample was washed with deionized water and alcohol several times to remove residual ions and molecules, and finally lightly dry it with N_2 for repeated use.

3. Results and discussion

3.1 Substrate characterization and spectroscopic measurements

The crystalline dendrite was fabricated by reducing Sn^{2+} in the $SnCl_2$ solution on Al substrate. In this study, we displace Sn^{2+} in solution with aluminum to form tin dendritic micro-nano structures on the Al matrix. The formation of dendritic tin fractal nanostructures was investigated by adjusting the reaction time. Wenzhao Jia *et al.* fabricated the Tin nanodendrites by using galvanic replacement reaction between stannous chloride ($SnCl_2$) and thermal evaporated zinc film composed of Zn nanodiscs.[28] As the reaction time increases, the color of the aluminum surface changes from silvery white to dark gray, and finally to black with fine silver-white crystals. H_2 will be generated during the entire reaction. The following is the chemical equation in the reaction:

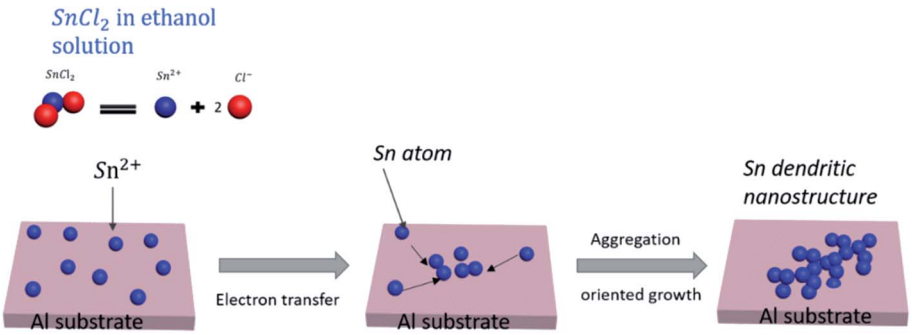

Fig. 1 Schematic diagram of the formation of tin branch nanostructures.

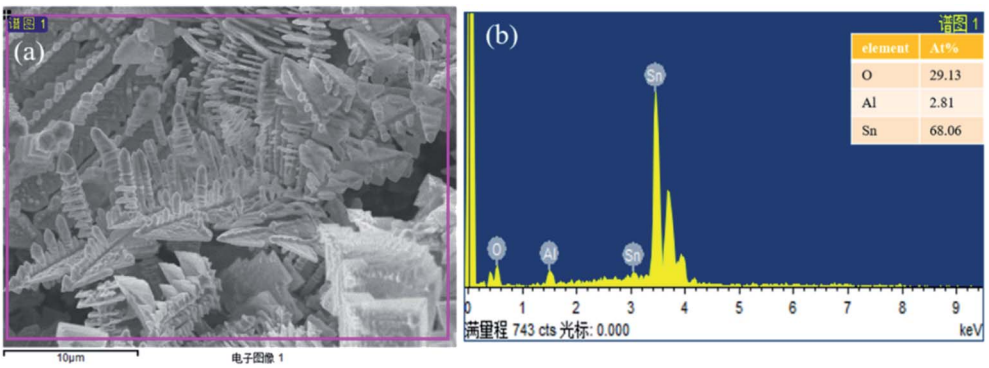

Fig. 2 (a) SEM images of tin dendritic nanostructures prepared for 7 min, (b) the EDS analytical energy spectrum of tin dendritic with 7 min reaction time.

$$Al + Sn^{2+} \rightarrow Sn + Al^{3+} \quad (1)$$

$$Al + CH_3CH_2OH \rightarrow (CH_3CH_2O)_3Al + H_2\uparrow \quad (2)$$

$$Sn^{2+} + 2e^- = Sn,\ E^0 = -0.140\ V \quad (3)$$

$$Al^{3+} + 3e^- = Al,\ E^0 = -1.662\ V \quad (4)$$

It has been reported that in the preparation of silver dendritic structure using displacement reaction *via* Zn and $AgNO_3$, under high silver ion concentration, strong anisotropic growth helps to form fine single crystal silver dendrites.[29] Dendritic nanostructures are products formed under non-equilibrium conditions, and their morphology sets the properties of many metallic alloys, the dendrites grow into a supersaturated liquid and the growth is by solute diffusion the dendrite growth dynamics during the free-growth stage are diffusion limited.[30] As the displacement reaction progress, the continuous growth of tin dendrites will deplete the monomer concentration in certain area. The Sn^{2+} ion concentration around previous grains drops to a certain level, small particles may have enough time to relax and grow oriented at the top part. In this paper, aluminum is more active as a reducing agent to reduce Sn^{2+} in the solution, hydroxyl hydrogen atoms in ethanol molecules will be replaced by aluminum, and generating hydrogen bubbles on the surface of aluminum. As the reaction progress, more and more tin atoms will accumulate on the Al surface, and hydrogen bubbles are constantly being produced. From the viewpoint of electrochemistry, there are two competitive reactions (Sn^{2+} reduction and H_2 evolution). The Al substrate is artificially polished, and the roughness of the surface will also have a certain effect on the growth of dendrites. Fig. 2 shows the SEM morphology and the elemental composition of tin dendritic nanostructures prepared for 7 min. It can be observed that the Al substrate was covered with tin dendrites. The tin dendritic nanostructures are composed of multilevel branch structures, which generates large area stalactite-like morphology on Al surface.

The tin dendrites grew from square particles to highly branched dendritic nanostructures during morphological evolution, as shown in Fig. 3. When the reaction time is 1 min, Sn atoms are initially nucleated. It can be clearly to see the grinding marks on the aluminum substrate and the protruding square Sn particles growing on the aluminum surface, the nucleation grows on the surface of aluminum and is relatively dispersed in Fig. 3(a). The size of the Sn block structure is about 2 μm, similar to a tree stump structure. The bubbles greatly suppress the splitting and growth of additional branches by concealing growth sites for the branches, if the bubbles are small, it can promote the vertical growth of dendritic nanostructures and inhibit the formation of side branches.[31,32] After 2 min reaction time, the reaction rate accelerated, and the initially grown tin nanoflowers with small particles propagated into thin rods as shown in Fig. 3(b). Long main stems and small branches can be observed. The size of the long main stem is about 5 microns, and the size of the small branches is 500 nm. When reaction time increased to 3 min, feather-like structure increases and formed hoarfrost-like large-area structures as shown in Fig. 3(c). Multiple flat main stems overlap each other, and multiple thin branches grow vertically on the main stem, and dendritic nanostructures are numerous and dense, forming a three-dimensional structure. When the reaction time increased to 5 min, a stepped folded structure is formed, the flat structure grows and expands laterally, and the square stacked structure perpendicular to its surface also grows slowly, as shown in Fig. 3(d). When reaction time increased to 7 min, high dendritic differentiation occurred, large complicated symmetrical tin dendritic were formed, and large-scale dendritic nanostructures grow into thin leaf-like flat structures, and there are a large number of square-shaped accumulations on the veins and surfaces of leaf branches (shown in insets), as shown in Fig. 3(e). In the reaction stage, the hydrogen bubble generation rate increases with the increase of the reaction time. After a certain period of time, the shape of the hydrogen bubble becomes larger, causing the dendritic structure to break and fall off on the aluminum substrate, when the reaction time was extended, the leaves became enlarged and collapsed as shown in Fig. 3(f).

It is found that the growth rate, morphology and structure of dendritic nanostructures are critical depended on the concentration of the reaction solution, reaction rate and reaction time.[33] Here, by controlling the experimental

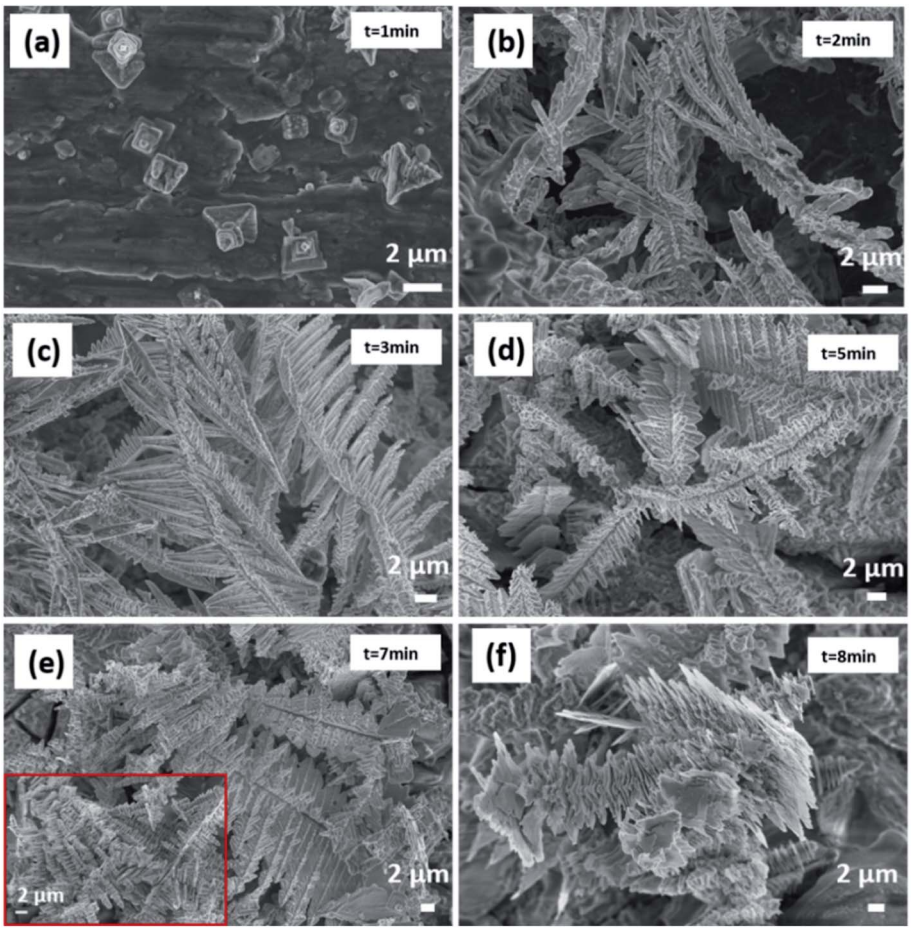

Fig. 3 SEM images of tin dendritic nanostructures prepared for (a) 1 min, (b) 2 min, (c) 3 min, (d) 5 min, (e) 7 min, (f) 8 min. The insets show the high magnification SEM image of tin dendritic nanostructures.

condition, such as the reaction solution concentration, reaction time and so on, and the growth mechanism of tin dendritic nanostructures was investigated. It is found that with the increasing the reaction time, the size of the hydrogen bubbles increases, the tin dendritic nanostructures are easily broken. J. C. Millare. *et al.*[34] reported that the addition of salt to the ethanol–water mixture solution will cause the anions to interact with the ethanol molecules, which will accumulate in the gas phase, resulting in an increase in bubble size. The solvent in the displacement reaction will significantly affect the reaction kinetics, thereby affecting the morphology of the product. It was found that the metal matrix, the ratio of ethanol and water and additives have a significant effect on the morphology of the obtained dendrites.[36] S. P. Xie *et al.*[35] reported the fast growth synthesis of silver dendrite based on a electroless galvanic displacement reaction between solid Cu and Ag(I) ion, and the influence of different anions (SO_4^{2-}, NO_3^-) in the solute on the morphology and structure of silver branches is investigated. As a result, for the stability of the tin dendritic structure, additives can be added during the reaction to suppress or reduce the generation of hydrogen bubbles, and the solute and solvent can also be changed to obtain a structure with better performance.

3.2 SEF activities of tin dendritic nanostructures

In order to investigate the regulation of tin dendritic nanostructures with different morphologies on the fluorescence spectrum we used rhodamine as a probe molecule and excited by a 532 nm laser, the aluminum substrate and the sample are treated in the same way during the test. The fluorescence spectrum of the Rh6G absorbed on the pure Al substrate was selected as a reference to inspect the SEF enhancement of tin branched dendritic nanostructure. As shown in Fig. 4, the fluorescence intensity of Rh6G deposited on the substrate gradually increased with the formation of the dendrites. However, when the reaction time was more than 8 min, the dendritic nanostructure collapsed, and the corresponding spectrum of Rh6G was weaker than that obtained from 7 min reaction time.

Metal nanostructures can adjust the SPR band and local field enhancement frequency through the size, shape and environment of the particles, but the absorption or emission bands of the dye are relatively fixed.[37] Due to the change of reaction time, the morphology of tin branches also changes significantly, the fluorescence spectra of Sn dendritic generated at different reaction times after the immersion of different Rh6G concentrations are shown in Fig. 4(a–d). The concentration of

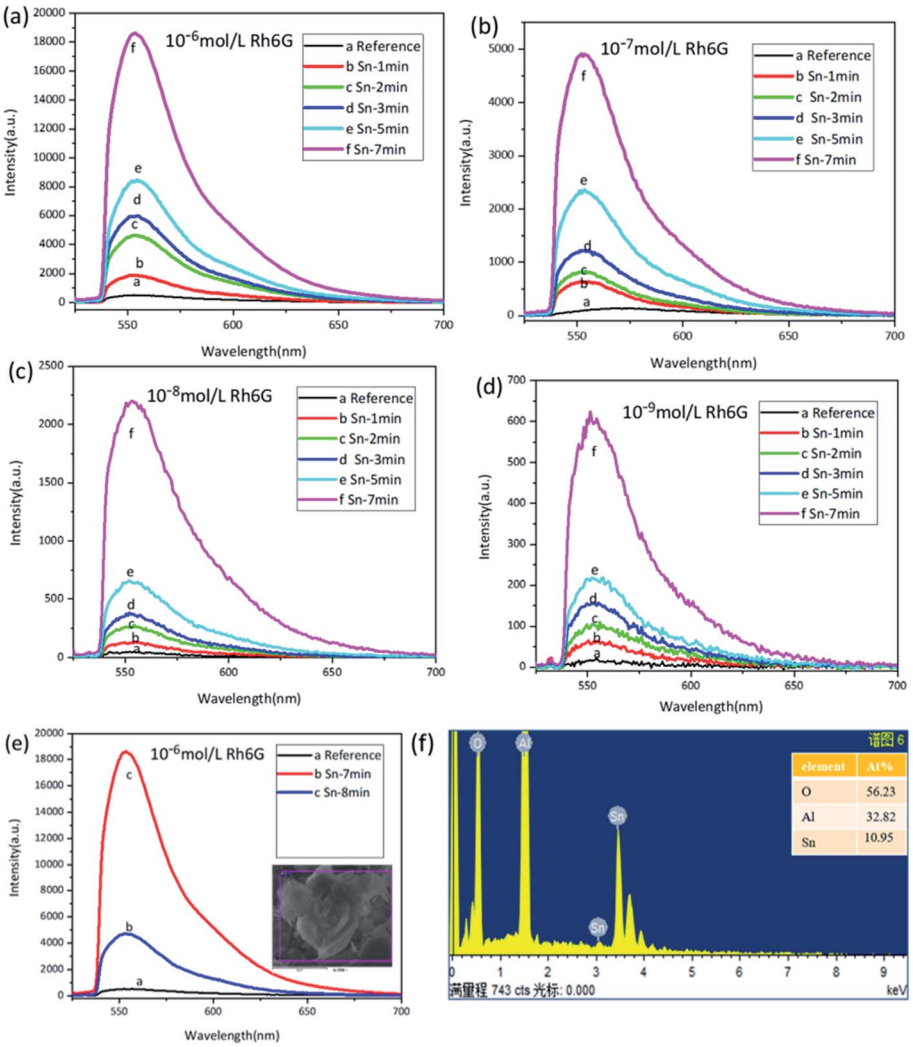

Fig. 4 Enhanced fluorescence spectra of Rh6G molecules deposited on various tin dendritic nanostructures (a) 10^{-6} mol L^{-1}, (b) 10^{-7} mol L^{-1}, (c) 10^{-8} mol L^{-1}, (d) 10^{-9} mol L^{-1}. (e) Is the fluorescence spectrum of tin dendritic corresponding to Rh6G concentration of 10 generated by 8 min reaction time; (f) is the EDS analytical energy spectrum of the insets in (e) that tin dendritic with 8 min reaction.

rhodamine molecules affects the number of fluorescent molecules deposited on the surface of the sample, resulting in different fluorescence intensities. The intensity of the fluorescence spectrum increases with time during the sample reaction time of 1 to 7 minutes. Fig. 4(e) shows the comparative spectra of tin dendrites at 7 min and 8 min. Compared with that at 8 min, the tin dendritic nanostructure prepared with 7 min reaction time has higher density and stable structure with excellent spectral intensity Fig. 4(f) is EDS analytical energy spectra of tin dendrites with 8 min reaction times.

By comparing the peak at 558 nm from the prepared metal substrates with that from the polished aluminum substrate in Fig. 4, the enhancement factor (EF) was proposed to express the enhanced fluorescent effects of tin branched dendritic nanostructure and was estimated through the following equation:[38]

$$EF = (I_{sample} - I_{background})/(I_{reference} - I_{background}) \quad (5)$$

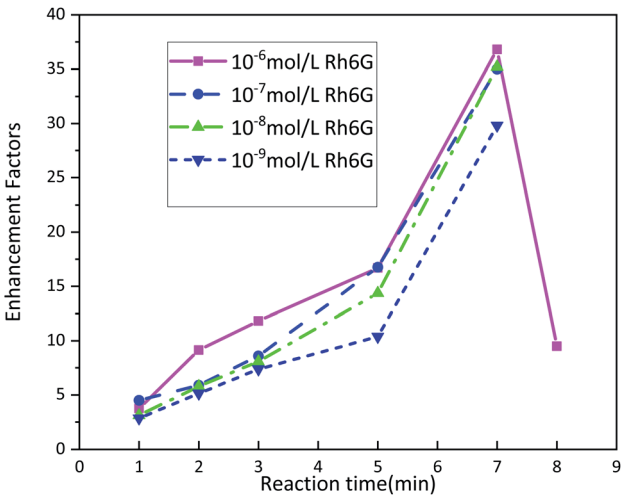

Fig. 5 Fluorescence enhancement factors of Rh6G molecules deposited on tin dendritic substrate with different concentration.

where I_{sample} and $I_{reference}$ are the SEF spectrum intensities of measured substrate, and $I_{background}$ is the environmental background light intensity. Under the same conditions, the SEF intensity with Rh6G solutions of 10^{-6}, 10^{-7}, 10^{-8}, and 10^{-9} mol L^{-1} concentrations was measured and is shown in Fig. 5.

According to the fluorescence spectrum experimental data, the tin dendritic nanostructure exhibited fluorescence enhancement as shown in Fig. 5. Seven spectrum detection points on each sample were randomly selected to investigate the sample homogeneity under high magnification microscope. The EF critically depends on the reaction time of substrate. With the increase in reaction time, the EF value also increased. However, when the reaction time was longer than 7 min, the dendritic nanostructure had collapsed and reduced the fluorescence enhanced effect. Rh6G solution (10^{-6} mol L^{-1}) was selected as the sample immersion solution. Under reaction times of 1, 2, 3, 5, 7, and 8 min, the EF was 3.75, 9.15, 11.82, 16.69, 36.81, and 9.50, respectively. With different Rh6G solution concentrations, the fluorescence EF reached an highest value at 7 min reaction time. When beyond this duration, EF value will be decreased. The metallic nanostructures and metallic colloidal nanoparticles interact with the proximal fluorophore and produce higher quantum yields.[39] Experimental observations show that the fluorescence enhanced ability of the sample surface is strongly correlated with the sample morphology. The morphology of tin dendritic nanostructures formed under 7 min reaction time exhibits the best fluorescence enhancement effect. Careful examination of SEM revealed that the tin branched dendritic nanostructures had large-area stacked complex structures may be conducive to the absorption of Rh6G molecules. In particular, when metal dendrites were excited by an external light field, local field enhancement is generated at the end of branches, and young twigs can become needle tips that positively influence local EM field. In addition, strong EM coupling can occur in the space between two adjacent branches from the coupling of SPR and the nanogap formed in the nanostructures has a crucial role in enhancing the local EM field,[40,41] the electromagnetic field intensity of these hotspots is much higher than other locations, resulting in strong fluorescence signals from nearby fluorophore molecules. As a result, the tin dendritic nanostructure exhibiting fluorescence enhanced efficiency.

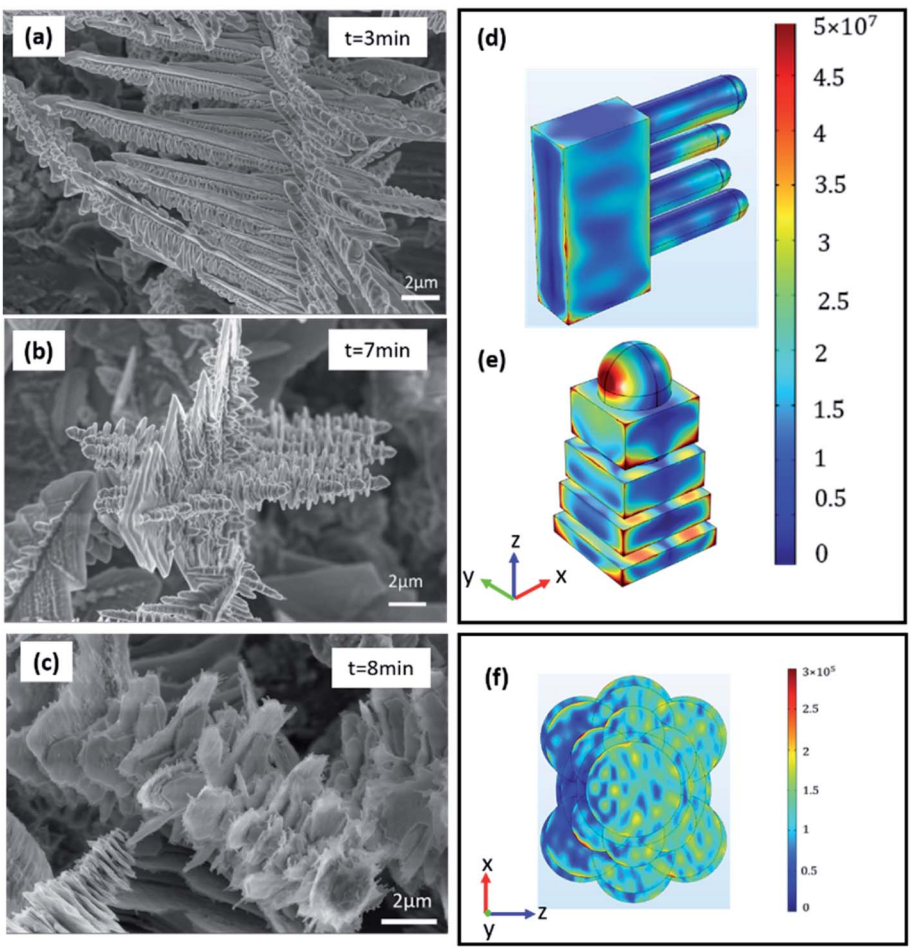

Fig. 6 Higher magnification scales SEM images of tin dendritic nanostructures prepared for (a) 3 min, (b) 7 min, (c) 8 min, (d) 5 min,correspondingly, construct simulated tin branch nanostructures (d–f).

The EM field distributions of tin dendritic nanostructures on a planar surface were calculated using finite element method (FEM). The simulation model is based on the SEM picture of tin nanostructure as shown in Fig. 6(a–c). Select the characteristic parts of tin branches of different shapes and compare their electric field distributions. Fig. 6(d) and (e) show the spatial distribution of electric field for local EM fields were generated in the tin dendrites of gaps and adjacent dendrite structures excited *via* the 532 nm laser with *Y* polarization from *Z* axis. Strong EM "hot spots" were produced in the nanogap and tip. The strong electric field is distributed in the space between two adjacent branches as shown in Fig. 6(d). As seen in Fig. 6(e), the EM field was enhanced in the nanogap formed from the accumulation of small squares on tin dendrites. The highest enhancement of electric field was found at the top of the branch nanostructure. At the same electromagnetic scale, compared with branched and nano-gap structures, large blade-shaped structures have very weak electromagnetic field enhancement at the edge of the blade, changing the electromagnetic scale can better observe the part of electromagnetic enhancement as shown in Fig. 6(f). This simulation proves that the formed "hot spots" between the tip and nanogap are dedicated to generating surface plasmons and local EM field. In addition, the fluorescence signal was dramatically enhanced when the tin dendritic nanostructure was formed.

4. Conclusion

Tin dendritic nanostructure substrates with controllable morphology were prepared through *in situ* replacement without surfactant. The growth mechanism of tin dendritic nanostructures has been proposed. Under 532 nm laser excitation, the tin dendritic nanostructures can detect 10^{-9} mol L^{-1} Rh6G, and fluorescence enhancement can reach 29.81-fold that on pure Al substrate. Theoretical analysis proves that the large number of "hot spots" generated in tin dendritic nanostructures provide an advantage to excite surface plasmon resonance. Furthermore, local enhanced EM field excited among the dendritic nanostructures was observed based on FEM simulation. In this work, a simple, convenient, and low-cost method was used to fabricate tin dendritic nanostructure with fluorescence enhancement capability. This study provides reliable experimental support for fluorescence enhancement with great potential in SEF investigation.

Conflicts of interest

There are no conflicts to declare.

Acknowledgements

The Shaanxi Province International Cooperation and Exchange Program (Grant No. 2019KW-027), Natural Science Foundation of Shaanxi Provincial (Grant No. 2018JQ6009), Shaanxi Provincial Research Plan for Young Scientific and Technological New Stars (Grant No. 2019KJXX-058), Xi'an University of Posts and Telecommunications Joint Postgraduate Cultivation Workstation (Grant No. CXJJLY2018057), and Xi'an University of Posts and Telecommunications Joint Postgraduate Cultivation Workstation (YJGJ201905).

References

1 Z. G. Dai, X. H. Xiao, W. Wu, Y. P. Zhang, L. Liao, S. S. Guo, J. J. Ying, C. X. Shan, M. T. Sun and C. Z. Jiang, Plasmon-driven reaction controlled by the number of graphene layers and localized surface plasmon distribution during optical excitation, *Light Sci. Appl.*, 2015, **4**, e342.

2 Y. Yin, P. Miao, Y. M. Zhang, J. C. Han, X. H. Zhang, Y. Gong, L. Gu, C. Y. Xu, T. Yao, P. Xu, Y. Wang, B. Song and S. Jin, Significantly Increased Raman Enhancement on MoX_2 (X = S, Se) Monolayers upon Phase Transition, *Adv. Funct. Mater.*, 2017, **27**, 1606694.

3 J. Xu, C. H. Li, H. P. Si, X. F. Zhao, L. Wang, S. Z. Jiang, D. M. Wei, J. Yu, X. W. Xiu and C. Zhang, 3D SERS substrate based on Au-Ag bi-metal nanoparticles/MoS_2 hybrid with pyramid structure, *Optics express*, 2018, **26**(17), 21546–21557.

4 H. Zong, X. Wang, X. Mu, J. Wang and M. Sun, Plasmon-Enhanced Fluorescence Resonance Energy Transfer, *Chem. Rec.*, 2019, **19**, 818–842.

5 X. Zhao, J. Dong, E. Cao, Q. Han, W. Gao, Y. Wang, J. Qi and M. T. Sun, Plasmon-exciton coupling by hybrids between graphene and gold nanorods vertical array for sensor, *Appl. Mater. Today.*, 2019, **14**, 166–174.

6 S. E. Wang, Y. Huang, K. Hu, J. Tian and S. L. Zhao, A highly sensitive and selective aptasensor based on fluorescence polarization for the rapid determination of oncoprotein vascular endothelial growth factor (VEGF), *Anal. Methods*, 2014, **6**(1), 62–66.

7 C. Fan, X. Lv, F. Liu, L. Feng, M. Liu, Y. Cai, H. Liu, J. Wang, Y. Yang and H. Wang, Silver nanoclusters encapsulated into metal–organic frameworks with enhanced fluorescence and specific ion accumulation toward the microdot array-based fluorimetric analysis of copper in blood, *ACS Sens.*, 2018, **3**(2), 441–450.

8 J. Yang, A. Moraillon, A. Siriwardena, R. Boukherroub, F. Ozanam, A. Chantal Gouget-Laemmel and S. Szunerits, Carbohydrate microarray for the detection of glycan–protein interactions using metal-enhanced fluorescence, *Anal. Chem.*, 2015, **87**(7), 3721–3728.

9 N. Sui, L. Wang, F. Xie, F. Liu, H. Xiao, M. H. Liu and W. W. Yu, Ultrasensitive aptamer-based thrombin assay based on metal enhanced fluorescence resonance energy transfer, *Microchim. Acta*, 2016, **183**(5), 1563–1570.

10 K. Sugawa, T. Tamura, H. Tahara, D. Yamaguchi, T. Akiyama, J. Otsuki, Y. Kusaka, N. Fukuda and H. Ushijima, Metal-enhanced fluorescence platforms based on plasmonic ordered copper arrays: wavelength dependence of quenching and enhancement effects, *ACS Nano*, 2013, **7**(11), 9997–10010.

11 J. Dong, Z. L. Zhang, H. R. Zheng and M. T. Sun, Recent progress on plasmon-enhanced fluorescence, *Nanophotonics*, 2015, **4**(1), 472–490.

12 Y. Zhang, C. L. Yang, X. J. Xiang, P. G. Zhang, Z. H. Peng, Z. L. Cao and L. Xuan, Highly effective surface-enhanced fluorescence substrates with roughened 3D flowerlike silver nanostructures fabricated in liquid crystalline phase, *Appl. Surf. Sci.*, 2017, **401**, 297–305.

13 J. J. Wang and Z. H. Jia, Metal nanoparticles/porous silicon microcavity enhanced surface plasmon resonance fluorescence for the detection of DNA, *Sensors*, 2018, **18**(2), 661.

14 A. Lotfi, M. Nikkhah and A. Moshaii, Development of metal-enhanced fluorescence-based aptasensor for thrombin detection using silver dendritic nanostructures, *Plasmonics*, 2019, **14**(3), 561–568.

15 C. R. Simovski, M. S. M. Mollaei and P. M. Voroshilov, Fluorescence quenching by plasmonic nanoantennas, *Phys. Rev. B*, 2020, **101**, 245421.

16 A. M. Gabudean, M. Focsan and S. Astilean, Gold nanorods performing as dual-modal nanoprobes via metal-enhanced fluorescence (MEF) and surface-enhanced Raman scattering (SERS), *J. Phys. Chem. C*, 2012, **116**(22), 12240–12249.

17 Z. Zhang, J. Malicka, I. Gryczynski and J. R. Lakowicz, Surface-enhanced fluorescence of fluorescein-labeled oligonucleotides capped on silver nanoparticles, *J. Phys. Chem. B*, 2005, **109**(16), 7643–7648.

18 J. Zhu, K. Zhu and L. Huang, Using gold colloid nanoparticles to modulate the surface enhanced fluorescence of Rhodamine B, *Phys. Lett. A*, 2008, **372**(18), 3283–3288.

19 Y. Zhang, A. Dragan and C. D. Geddes, Metal-enhanced fluorescence from Tin nanostructured surfaces, *J. Appl. Phys.*, 2010, **107**(2), 024302.

20 O. Amiri, M. Salavati-Niasari, N. Mir, F. Beshkar, M. Saadat and F. Ansari, Plasmonic enhancement of dye-sensitized solar cells by using Au-decorated Ag dendrites as a morphology-engineered, *Renewable energy*, 2018, **125**, 590–598.

21 L. Liu, K. Zhuo, Z. Yuan, Q. Zhang, W. Zhang and S. Sang, Nano-branched Silver Dendrites Modified Glassy Carbon Electrode for Detection of Heavy Metal Ions, *Int. J. Electrochem. Sci.*, 2019, **14**, 5317–5330.

22 X. X. Wang, D. D. Yang, L. Z. Chen, B. Liu, Z. G. Teng, N. Y. He and Z. F. Wang, 2D Dendritic Gold Nanostructures Formed on Silica Nanosheets: Transferability, Clean Surface, and Their Biomedical Application, *Part. Part. Syst. Char.*, 2018, **35**(10), 1800268.

23 G. Xing, K. Wang, P. Li, W. Q. Wang and T. Chen, 3D hierarchical Ag nanostructures formed on poly (acrylic acid) brushes grafted graphene oxide as promising SERS substrates, *Nanotechnology*, 2018, **29**(11), 115503.

24 L. H. Lu, A. Kobayashi, Y. Kikkawa, K. Tawa and Y. Ozaki, Oriented attachment-based assembly of dendritic silver nanostructures at room temperature, *J. Phys. Chem. B*, 2006, **110**(46), 23234–23241.

25 W. Q. Zhang, J. Liu, W. X. Niu, H. Yan, X. M. Lu and B. Liu, Tip-Selective Growth of Silver on Gold Nanostars for Surface-Enhanced Raman Scattering, *ACS Appl. Mater. Interfaces*, 2018, **10**(17), 14850–14856.

26 J. Dong, S. X. Qu, H. R. Zheng, Z. L. Zhang, J. N. Li, Y. P. Huo and G. A. Li, Simultaneous SEF and SERRS from silver fractal-like nanostructure, *Sensor. Actuator. B Chem.*, 2014, **191**, 595–599.

27 A. Parfenov, I. Gryczynski, J. Malicka, C. D. Geddes and J. R. Lakowicz, Enhanced fluorescence from fluorophores on fractal silver surfaces, *J. Phys. Chem. B*, 2003, **107**(34), 8829–8833.

28 W. Z. Jia, L. Su, X. P. Li, L. C. Zhang, Z. Y. Gu, P. X. Gao and Y. Lei, Synthesis of tin nanodendrites via galvanic replacement reaction and their thermal conversion to nanodendritic tin oxide for ultrasensitive electrochemical sensing, *RSC Adv.*, 2011, **1**(8), 1500–1505.

29 J. X. Fang, H. J. You, P. Kong, Y. Yi, X. P. Song and B. J. Ding, Dendritic silver nanostructure growth and evolution in replacement reaction, *Cryst. Growth Des.*, 2007, **7**(5), 864–867.

30 J. W. Gibbs, K. A. Mohan, E. B. Gulsoy, A. J. Shahani, X. Xiao, C. A. Bouman, M. De Graef and P. W. Voorhees, The three-dimensional morphology of growing dendrites, *Sci. Rep.*, 2015, **5**(1), 1–9.

31 C. L. Wang, C. S. Lin, Y. Hwu, C. H. Chen, L. Chang, H. Je and G. Margaritondo, Hydrogen bubbles and the growth morphology of ramified zinc by electrodeposition, *J. Electrochem. Soc.*, 2008, **155**(5), D400.

32 T. Kim, K. Hong, D. Sohn, M. Kim, D. Nam, E. Cho and H. Kwon, One-step synthesis of multilayered 2D Sn nanodendrites as a high-performance anode material for Na-ion batteries, *J. Mater. Chem. A*, 2017, **5**(38), 20304–20315.

33 J. S. Yang and Z. D. Jiang, Facile fabrication of dendritic silver structures and their surface enhanced Raman spectroscopic properties, *J. Chem. Sci.*, 2015, **127**(1), 173–176.

34 J. C. Millare and B. A. Basilia, Nanobubbles from Ethanol-Water Mixtures: Generation and Solute Effects via Solvent Replacement Method, *ChemistrySelect*, 2018, **3**(32), 9268–9275.

35 S. P. Xie, X. C. Zhang, D. Xiao, M. Chin Paau, J. Huang and M. M. F. Choi, Fast growth synthesis of silver dendrite crystals assisted by sulfate ion and its application for surface-enhanced Raman scattering, *J. Phys. Chem. C*, 2011, **115**(20), 9943–9951.

36 X. T. Bai, Y. A. Gao and L. Q. Zheng, Galvanic replacement mediated growth of dendritic gold nanostructures with a three-fold symmetry and their applications to SERS, *CrystEngComm*, 2011, **13**(10), 3562–3568.

37 J. Zhu, K. Zhu and L. Q. Huang, Using gold colloid nanoparticles to modulate the surface enhanced fluorescence of Rhodamine B, *Phys. Lett. A*, 2008, **372**(18), 3283–3288.

38 J. Dong, H. Zheng, X. Yan, Y. Sun and Z. Zhang, Fabrication of flower-like silver nanostructure on the Al substrate for surface enhanced fluorescence, *Appl. Phys. Lett.*, 2012, **100**(5), 051112.

39 Y. Jeong, Y. Kook, K. Lee and W. Koh, Metal enhanced fluorescence (MEF) for biosensors: general approaches and

a review of recent developments, *Biosens. Bioelectron.*, 2018, **111**, 102–116.

40 Z. Q. Cheng, Z. W. Li, J. H. Xu, R. Yao, Z. L. Li, S. Liang, G. Cheng, Y. Zhou, X. Luo and J. Zhong, Morphology-controlled fabrication of large-scale dendritic silver nanostructures for catalysis and SERS applications, *Nanoscale Res. Lett.*, 2019, **14**(1), 1–7.

41 H. J. Yin, Z. Y. Chen, Y. M. Zhao, M. Y. Lv, C. N. Shi, Z. L. Wu, X. Zhang, L. Liu, M. L. Wang and H. J. Xu, Ag@Au core-shell dendrites: a stable, reusable and sensitive surface enhanced Raman scattering substrate, *Sci. Rep.*, 2015, **5**, 14502.

